Available online at www.sciencedirect.com
ScienceDirect
Journal of Molecular Catalysis A: Chemical 272 (2007) 275–287
JOURNAL OF MOLECULAR CATALYSIS A: CHEMICAL
www.elsevier.com/locate/molcata

What is the product of ketene hydrogenation on $Fe_5C_2(0\,0\,1)$: Oxygenates or hydrocarbons?

Dong-Bo Cao [a], Sheng-Guang Wang [a], Yong-Wang Li [a], Jianguo Wang [a], Haijun Jiao [a,b,*]

[a] *State Key Laboratory of Coal Conversion, Institute of Coal Chemistry, Chinese Academy of Sciences, Taiyuan 030001, PR China*
[b] *Leibniz-Institut für Katalyse e.V. an der Universität Rostock e.V., Albert-Einstein-Strasse 29a, 18059 Rostock, Germany*

Received 10 October 2006; received in revised form 17 March 2007; accepted 21 March 2007
Available online 27 March 2007

Abstract

Density functional theory calculations have been carried out on the reaction of ketene hydrogenation on $Fe_5C_2(0\,0\,1)$ for the understanding of the Fischer–Tropsch synthesis mechanism. The main reaction pathway of ethene formation is $C_sH_2CO \rightarrow CC_sH_2 \rightarrow CHC_sH_2 \rightarrow CH_2C_sH_2$, and ethane formation follows $C_sH_2CO \rightarrow CC_sH_2 \rightarrow CC_sH_3 \rightarrow CC_sH_3 \rightarrow CHC_sH_3 \rightarrow CH_2C_sH_3 \rightarrow CH_3C_sH_3$, while that of ethanol is $C_sH_2CO \rightarrow$ [C_sH_3CO and/or C_sH_2CHO] $\rightarrow C_sH_3CHO \rightarrow C_sH_3CH_2O \rightarrow C_sH_3CH_2OH$. Detailed comparison shows clearly that ketene dissociation with the formation of hydrocarbons is more favorable than the stepwise hydrogenation with the formation of ethanol. The expected product should be hydrocarbons rather than ethanol, in agreement with the experimental observation.

Keywords: Fe_5C_2; Ketene hydrogenation; Fischer–Tropsch synthesis; DFT

1. Introduction

Fischer–Tropsch synthesis (FTS) is a complex catalytic process that converts syngas (CO and H_2) into linear paraffins and α-olefins as major products and a few oxygenated byproducts. In order to understand FTS, many reaction mechanisms were proposed such as the carbide mechanism [1,2] and the CO insertion mechanism [3]. The carbide mechanism can explicitly explain the formation of hydrocarbons, but fails to explain the oxygenated products. For the CO insertion mechanism, CO inserts into surface alkyl and this forms oxygen-containing intermediates, which further result in hydrocarbons and oxygenates. Kummer and Emmett [4] and Berziger and Madix [5] studied the addition of radioactive alcohols on iron catalysts, and found that alcohol-related intermediates can lead to the formation of hydrocarbons in FTS.

Ketene ($H_2C{=}C{=}O$) has been considered as a principal intermediate for C_2 hydrocarbons and oxygenates in FTS [6]. On the basis of X-ray photoelectron spectroscopy [7], two routes for ketene formation on Fe have been proposed, (i) CO insertion into a surface carbene ($H_2C_s + CO \rightarrow H_2C{=}C{=}O$) and (ii) CO insertion into a surface carbon to form ketenylidene followed by hydrogenation ($C_s + CO \rightarrow C{=}C{=}O \rightarrow H_2C{=}C{=}O$). Ketenylidene as ligand has been observed in metal carbonyl complex $[Fe_3(CO)_9(CCO)]^{2-}$ [8]. Recent theoretical study on the adsorption of CO and H_2 on $Fe_5C_2(0\,0\,1)$ and $Fe_5C_2(1\,1\,0)$ showed the formation of surface ketenylidene from CO insertion into surface carbon [9] and the formation of surface ketene by ketenylidene hydrogenation [10]. A recent in situ infrared study of CO adsorption on fresh-prepared β-Mo_2C showed the existence of ketenylidene [11], and this result is confirmed by density functional theory (DFT) calculation on CO adsorption on C-terminated Mo_2C surface with ketenylidene as the most stable surface species [12].

Ketene hydrogenation results in ethanol. For ethanol formation on cobalt carbonyls, Daroda et al. [13] proposed the carbene → ketene → ethanol route. Takeuchi and Katzer [14] studied ethanol formation from H_2 and $^{12}C^{18}O/^{13}C^{16}O$ on Rh/TiO_2, and proposed the mechanism in favor of CO insertion into carbene instead of methyl group on the basis of the isotopic distribution. However, Deluzarche et al. [15] found that the isotopic distribution by Takeuchi et al. [14] could also be compatible with the mechanism consisting of CO insertion into a methyl group using $H_2{}^{16}O/H_2{}^{18}O$. Using infrared spectroscopic

* Corresponding author. Tel.: +49 3811281135; fax: +49 38112815000.
E-mail address: haijun.jiao@catalysis.de (H. Jiao).

1381-1169/$ – see front matter © 2007 Elsevier B.V. All rights reserved.
doi:10.1016/j.molcata.2007.03.057

techniques Fukushima et al. observed surface acetyl (CH_3CO), ethoxy (CH_3CH_2O) as intermediates in ethanol formation on Rh–Fe/SiO_2 at 503 K [16] and on Rh/SiO_2 at 503–543 K [17].

Apart from ketene hydrogenation into ethanol, C–O cleavage can occur and lead to hydrocarbons. Henderson et al. studied ketene hydrogenation on Ru(0 0 1) and found acetaldehyde (CH_3CHO), acetyl (CH_3CO) and ethylidyne (CCH_3) at 200–250 K, or ethylidyne at 350 K as main intermediates by using static secondary ion mass spectroscopy and temperature programmed desorption [18,19]. Furthermore, it shows experimentally that the main FTS products are C_2 hydrocarbons, while the yield of C_2 oxygenate is rather low [20,21].

Formation of C_2 hydrocarbons and C–C coupling mechanism are widely studied previously. For example, Liu and Hu [22] investigated C–C couplings on Ru(0 0 0 1) and Ru-step using the DFT method, and found that C + CH is the most favorable pathway resulting in ethylidyne (CCH_3), compared to other reactions (C + C, C + CH_2, CH + CH, CH + CH_2, CH_2 + CH_2, CH_2 + CH_3). Zheng et al. [23] investigated the coupling mechanism of CH_3 + CH_3, CH_3 + CH_2, CH_2 + CH_2 on Ti(0 0 0 1), Cr(1 1 0) and Co(0 0 0 1) using tight binding extend Hückel method, and found that the endothermicity decreases for CH_3 + CH_3 and CH_3 + CH_2 across the periodic table from left to right, and the corresponding reaction barriers also decrease, while CH_2 + CH_2 coupling reaction on these three surfaces is exothermic without barrier. For CH + CH_2 coupling reaction on Co(0 0 0 1) and Ru(0 0 0 1) [24], the reaction barrier on Co(0 0 0 1) is 0.63 eV, lower than on Ru(0 0 0 1), and the reaction is slightly exothermic on Co(0 0 0 1), but endothermic on Ru(0 0 0 1). Despite many theoretical studies on the formation of C_2 hydrocarbons, no study on the formation of C_2 hydrocarbons and oxygenates from CO and H_2 are reported.

As reported previously, CO insertion into the surface carbon on Fe_5C_2(0 0 1) forms surface ketene (η^3-C_s=C=O, **1**) [9]. Ketene hydrogenation leads to various oxygenated products and hydrocarbons. It is found that acetyl, acetaldehyde, ethoxy, and ethylidyne intermediates can exist on Rh–Fe/SiO_2 and on Ru(0 0 1) catalysts [13–19]. On the basis of ketene adsorption on Fe_5C_2(0 0 1) and on the fact of C–C and C–O bond cleavage of ethanol on Pt(1 1 1) [25], four possible elementary steps for ethanol formation by stepwise hydrogenation in Scheme 1 can be outlined: (a) formation of hydroxyvinyl (H_2C_s=C–OH, **2a**), acetyl (H_3C_s–C=O, **2b**) and formylmethyl (H_2C_s–CH=O, **2c**); (b) formation of hydroxyethylidene (H_3C_s–C–OH, **3a**), acetaldehyde (H_3C_s–CH=O, **3b**), and vinyl alcohol (H_2C_s=CH–OH, **3c**); (c) formation of 1-hydroxyethyl (H_3C_s–CH–OH, **4a**), ethoxy (H_3C_s–CH_2–O, **4b**) and 2-hydroxyethyl (H_2C_s–CH_2–OH, **4c**); (d) formation of ethanol (C_sH_3–CH_2–OH, **5**), respectively. During these processes, C–O cleavage of these important intermediates is also considered. For example, H addition to vinylidene (**6**), which is formed by ketene dissociation, can result in ethene and ethane formation. Thus, four possible elementary steps for ethane formation from vinylidene hydrogenation can also be outlined: (a) formation of ethylidyne (CC_sH_3, **7a**) and vinyl (CHC_sH_2, **7b**); (b) formation of ethylidene (CHC_sH_3, **8a**) and ethene ($CH_2C_sH_2$, **8b**); (c) formation of ethyl ($CH_2C_sH_3$, **9**); (d) formation of ethane ($CH_3C_sH_3$, **10**). Among them, ethylidyne (**7a**) was observed in experiments [18,19], while vinylidene (**6**) and vinyl (**7b**) are both related with chain propagation. Mims et al. [26–28] proposed surface vinylidyne as C_2 initiator, while Turner et al. [29–33] suggested surface vinyl as C_2 initiator.

For understanding ketene hydrogenation on Fe_5C_2(0 0 1), we investigated the thermodynamic and kinetic properties for these important elementary steps, and analyzed the main reaction pathway. Furthermore, the C_2 selectivity is elucidated.

2. Methods and models

Ketene hydrogenation was computed at the DFT level by using the Cambridge Sequential Total Energy Package (CASTEP) [34,35]. The exchange correlation energy was described with the Perdew–Burke–Ernzerhof (PBE) [36,37] form using generalized gradient approximation (GGA). Ionic cores were described by ultrasoft pseudopotential [38] and the Kohn–Sham one-electron states were expanded in a plane wave basis set up to 340 eV. The error of the adsorption energy of the oxygenated and hydrocarbon intermediates at the level of cutoff between 300 and 340 eV was less than 0.02 eV. A Fermi smearing of 0.1 eV was utilized. Brillouin zone integration was approximated by a sum over special k-points chosen using the Monhorst-Pack scheme [39]. The pseudopotential with partial core was used in spin-polarized calculations to include nonlinear core corrections [40]. Spin polarization was included for the super paramagnetic Fe_5C_2 [41] to correctly account magnetic properties. Spin polarization was also used to calculate

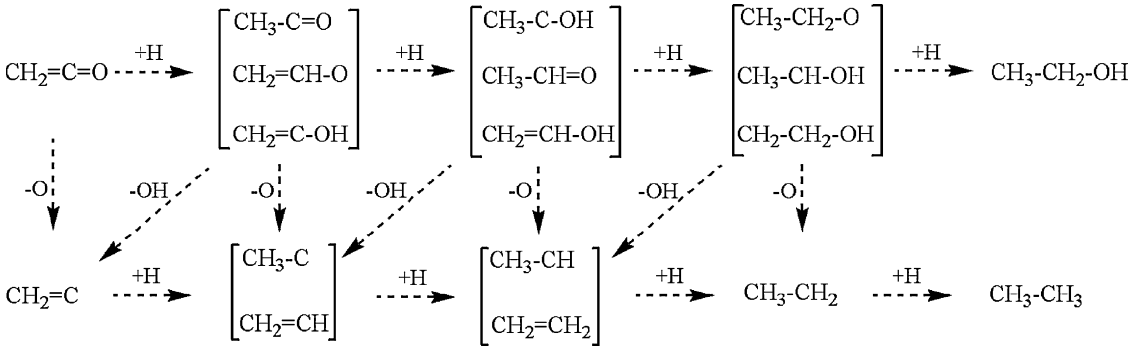

Scheme 1. Proposed elementary steps for ethanol and ethane formation.

the energies and structural parameters of the isolated radical species. Without counting the adsorbate, the vacuum between the slabs was set to span the range of 10 Å for the slabs without significant interaction. For ethane and ethanol formation, we used a model with a vacuum width of 12 Å, and found that the change in energy is less than 0.001 eV. The convergence criteria for structure optimization and energy calculation were 2.0×10^{-6} eV/atom for SCF, 2.0×10^{-5} eV/atom for energy, 0.05 eV/Å for maximum force, and 2.0×10^{-3} Å for maximum displacement. For checking the influence of force, we also performed calculations at the level of maximum force tolerance of 0.03 eV/Å. The resulted change of adsorption energies is less than 0.02 eV for **2a**–**c**, and **6** on Fe_5C_2(0 0 1). Transition states are calculated using the linear synchronous transit optimization methods [42]. The transition state structure is estimated by linear synchronous search from reactant and product, and followed by a conjugate gradient energy minimization in directions conjugate to the reaction pathway. Due to the irregularity of the Fe_5C_2 surfaces, the convergence criterion for transition state calculations was set to root-mean-square forces on atom tolerance of 0.25 eV/Å. It is to be noted that it is rather difficult to reach higher convergence criteria for transition states calculations. We used the *Molarch*+ program [43] for the molecular graphics.

The optimized Hägg iron carbide (Fe_5C_2) cell parameters agree with the experimental values [9,44]. The calculated magnetic moment for Fe_5C_2 is $1.79\mu_B$, in close agreement with the experimental value of $1.78\mu_B$ [45]. There are two terminations for Fe_5C_2(0 0 1), Fe–C termination and Fe-termination. The slab of Fe–C termination can be created from the Fe_5C_2 crystal structure, while the slab of Fe-termination can be created from the substrate of the outermost layer of the Fe–C termination slab (Fig. 1). There are other Fe–C termination slabs with the same stoichiometry of Fe and C atoms over the outermost layer. In order to maintain surface stoichiometry as much as possible and ensure inversion symmetry at the center of the slab, the Fe–C and Fe-termination slabs are exactly the thickness of integer-multiples of the bulk unit cell thickness. Vacuum thickness was set equal to the slab thickness for these two slabs. The surface energy was defined as: $E_{surf} = (E_{slab} - NE_{bulk})/2A$, where E_{slab} is the total energy of the slab, N is the number of Fe_5C_2 units in the slab, E_{bulk} is the bulk total energy per Fe_5C_2 unit, and A is the surface area of the slab. The Fe_5C_2 unit cell contains 20 Fe and 8 C atoms. For Fe_5C_2(0 0 1), and the two orthogonal surface unit

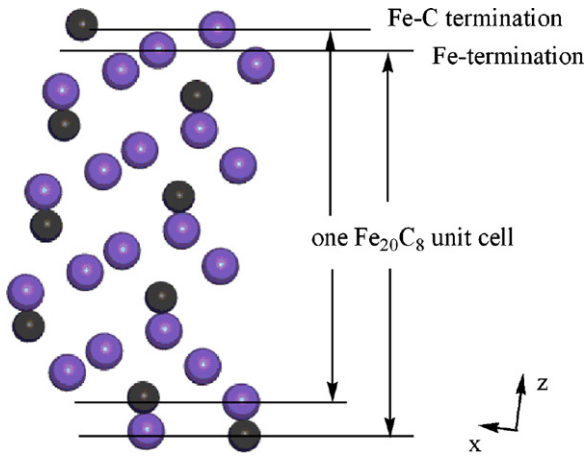

Fig. 1. Schematic side views of Fe–C termination and Fe-termination slab of Fe_5C_2(0 0 1).

cell lattice vectors (u and v) are 6.2167 and 4.5727 Å, respectively. The surface energies of unrelaxed stoichiometric Fe–C and Fe-termination slabs with one $Fe_{20}C_8$ unit cell thickness are 3.12 and 3.18 J/m^2, respectively. We also tested the surface energies of unrelaxed stoichiometric Fe–C and Fe-termination slabs with two $Fe_{20}C_8$ unit cell thicknesses (3.00 and 3.32 J/m^2, respectively). Due to the similar surface energies of slabs with one and two $Fe_{20}C_8$ unit cell thickness, the larger surface unit cells were not considered. For relaxed slabs with one $Fe_{20}C_8$ unit cell thickness, the surface energies of Fe–C and Fe-termination slab is 2.68 and 2.89 J/m^2, respectively, and the Fe–C termination slab is more stable than Fe-termination slab for the Fe_5C_2 (0 0 1) surface.

For the Fe–C termination of Fe_5C_2(0 0 1), we used a model system with five iron layers and three carbon layers (5Fe/3C), in which the bottom two iron layers and two carbon layers (2Fe/2C) are fixed in their bulk positions, while the three iron layers and one carbon layer on the top (3Fe/1C) are relaxed (Fig. 2). The top layer of Fe_5C_2(0 0 1) has both Fe and C in 1 to 1 ratio, while the second and third layers contain only Fe atoms. A $3 \times 5 \times 2$ k-grid sampling within the Brillouin zones was used in the p(1×1) unit cell. We also tested the k-point sampling by using the $4 \times 6 \times 2$ Monkhorst-Pack meshes for the unit cell, and the change in energy is less than 0.02 eV. In addition, a model system with seven iron layers and three carbon layers (7Fe/3C)

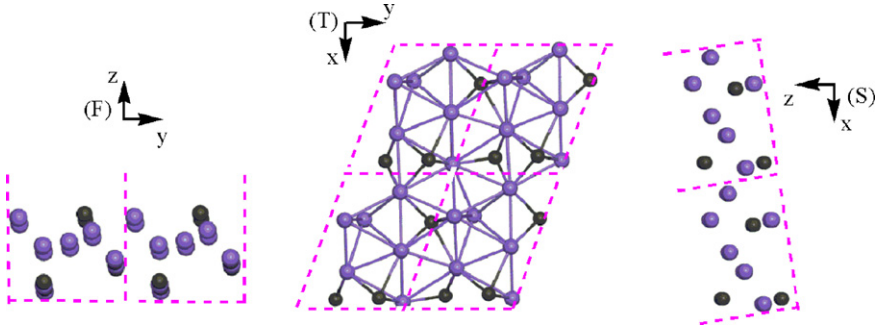

Fig. 2. Schematic top (T), front (F) and side (S) views of Fe_5C_2(0 0 1) in a p(1×1) unit cell. (purple: Fe atom; gray: C atom). (For interpretation of the references to colour in this figure legend, the reader is referred to the web version of the article.)

under the relaxation of the top four iron layers and two layer carbon layers (4Fe/2C) was tested, and the difference in adsorption energy of ketene (**1**) is only −0.01 eV. For lateral interaction, the adsorption energy of ketene (**1**) at 1/5 ML used by p(1 × 1) slab is −2.41 eV, while the adsorption energy of **1** at 1/10 ML used by p(1 × 2) and p(2 × 1) slabs is −2.41 and −2.43 eV, respectively, and the lateral interaction of ketene is very small. Similarly, the difference of the adsorption energies among **3a**–**c** at between 1/5 ML and 1/10 ML are less than ±0.05 eV. Thus, the p(1 × 1) slab was found to be sufficient for the ketene hydrogenation reactions.

Since surface carbon atom entered the intermediates and products, the adsorption energy of these species is defined as: $\Delta E_{ads} = E(\text{absorbate/slab}') - [E(\text{slab}') + E(\text{absorbate})]$, where E(absorbate/slab′) is the total energy for the slabs excluding surface carbon atom with adsorbate formed on the surface, E(slab′) is the total energy of the slab excluding surface carbon atom, and E(absorbate) is the total energies of free surface absorbate. The repulsion interaction of the co-adsorbed intermediates and H atoms is defined as: $E_{(rep)} = E_{(A+B)} + E_{(slab')} - (E_A + E_B)$. Since the repulsion energy of these co-adsorbed species is less than 0.2 eV, the total energy of these co-adsorbed surface species (A + B) is defined as: $E_{(A+B)} = E_A + E_B - E_{(slab')}$, and the energy barrier between the reactants and the transition state is defined as: $\Delta E = E_{TS} - E_{(A+B)}$.

3. Results and discussion

3.1. Adsorbed intermediates on surface

As shown in Fig. 3, the most stable surface ketene formed from CO addition to surface C_s atoms on Fe_5C_2(0 0 1) has an η^3 (C_s, C, O) bonding mode (**1**) with the strongest adsorption energy of −2.41 eV [10]. This is close to the adsorption energy of CO (−2.10 eV), but stronger than that (−0.90 eV) of H_2 on Fe_5C_2(0 0 1) [9,44]. The C–C and C–O bond lengths in **1** are 1.471 and 1.359 Å, respectively.

For ketene (**1**) hydrogenation, the adsorption energies and binding modes of the intermediates are shown in Table 1. On the basis of the adsorbed η^3 ketene structure in **1**, in which both C–C and C–O bonds are highly activated compared to free ketene, the adding hydrogen atom can bind at three different positions to result in the adsorbed hydroxyvinyl (H_2C_s=COH, **2a**), acetyl (H_3C_sC=O, **2b**) and formylmethyl (H_2C_s–CH=O, **2c**). As shown in Fig. 3 and Table 1, the most stable intermediate H_2C_s=C–OH (**2a**) has an η^3-bonding mode with the C–C and C–O bond lengths of 1.474 and 1.484 Å. In **2b** the adsorbed acetyl has an η^2-bonding mode with the C–C and C–O bond lengths of 1.490 and 1.360 Å. The least stable intermediate **2c** has an η^3-bonding mode with the C–C and C–O bond lengths of 1.454 and 1.382 Å. The computed adsorption energies of **2a**–**c** are −3.25, −2.66 and −2.43 eV, respectively.

The second H addition to **2b** can form hydroxyethylidene (H_3C–C–OH, **3a**) and acetaldehyde (H_3C–CH=O, **3b**), while H addition to **2c** can give acetaldehyde (H_3C–CH=O, **3b**) and hydroxyethylene (H_2C=CH–OH, **3c**). The optimized structures (**3a**–**c**) are shown in Fig. 3, and the adsorption energies are −2.59, −0.95, and −0.38 eV, respectively. **3a** has an η^2 (C, O) bonding mode with the C_s–C and C–O bond lengths of 1.497 and 1.581 Å. **3b** has an η^2 (C, O) bonding mode with the C_s–C and C–O bond lengths of 1.501 and 1.424 Å. **3c** has an η^3 (C_s, C, O) bonding mode with the C–C and C–O bond lengths of 1.465 and 1.430 Å.

In the third H addition step, hydrogen addition to **3a** leads to 1-hydroxyethyl (C_sH_3CHOH, **4a**), that to **3b** leads to **4a** and **b** (H_3C–CH_2–O), and that to **3c** leads to **4a** and **c**. The optimized structures (**4a**–**c**) are shown in Fig. 3, and the computed adsorption energies are −1.31, −2.85, and −1.35 eV, respectively. In this step, the least stable species is **4a** with an η^2 (C, O) bonding mode and the C_s–C and C–O bond lengths are 1.509 and 1.522 Å. The most stable intermediate $C_sH_3CH_2O$ (**4b**) has top site adsorption through O atom and the C–O bond length is 1.408 Å. In **4c** with an η^2 (C_s, O) bonding mode, the C–C and C–O bond lengths are 1.498 and 1.447 Å. Ethanol (**5**) is the final product of ketene hydrogenation. The adsorption energy of **5** is −0.51 eV. As shown in Fig. 7, only the O atom is bonded with a surface Fe atom, and the Fe–O bond length is 2.172 Å.

The dissociation of ketene may result in the formation of vinylidene (CC_sH_2) **6**. As shown in Fig. 4, the C atom of **6** is adsorbed at a four-fold site, and the absorption energy of **6** is −5.69 eV. Similarly, the adsorption energy of the three-fold CCH_2 fragment on Pt(1 1 1) is −5.85 eV [46]. The C–C bond length is 1.418 Å, and much longer than that of free CCH_2 radical by 1.275 Å. The hydrogenation of CC_sH_2 leads to the formation of CC_sH_3 and CHC_sH_2. The C atoms of **7a** and **7a′** are absorbed at four-fold and three-fold sites, and the adsorption energies of **7a** and **7a′** are −6.17 and −5.83 eV, respectively. In comparison, the adsorption energies of two-fold, and three-fold CCH_3 fragment on Pt(1 1 1) are −7.40 and −8.32 eV [46]. The CH of CHC_sH_2 in **7b** and **7b′** are absorbed at three-fold and four-fold sites, and the adsorption energies of **7b** and **7b′** are −3.00 and −3.51 eV, respectively. In comparison, the adsorption energy and C–C bond length of CH_2CH fragment on Ru(0 0 0 1) are −2.86 eV and 1.454 Å, respectively [24].

Further hydrogenation of CC_sH_3 (**7a**) and CHC_sH_2 (**7b**) forms CHC_sH_3 (**8a**) and $CH_2C_sH_2$ (**8b**), respectively. As shown in Fig. 4, the CH of **8a** is absorbed at a three-fold site, and the adsorption energy of **8a** is −3.75 eV. **8b** and **8b′** are di-σ adsorbed forms of ethene, while **8b″** is a π-adsorbed form of ethene. The adsorption energies of **8b**, **8b′** and **8b″** are −0.73, −0.97 and −0.93 eV, respectively. The C–C bond lengths are 1.497, 1.458 and 1.385 Å, respectively. In comparison, the most stable adsorbed form of ethene on Pt(1 1 1) is a di-σ form, with an adsorption energy of −1.13 eV and C–C bond length of 1.483 Å [47]. The hydrogenation of $CHCH_3$ (**8a**) and CH_2CH_2 (**8b**) can lead to the formation of CH_3CH_2 (**9**). The CH_2 of **9** is absorbed at a two-fold site, and the adsorption energy is −1.61 eV. The final product of ethyl hydrogenation is ethane (**10**), the adsorption energy of **10** is −0.07 eV.

3.1.1. Electronic factor

The local density of states (LDOS) of free and adsorbed CH_2COH (**2a**), CH_3CO (**2b**), and CH_2CHO (**2c**) are shown in Fig. 5. The valence bands of free **2a**–**c** as doublet ground state

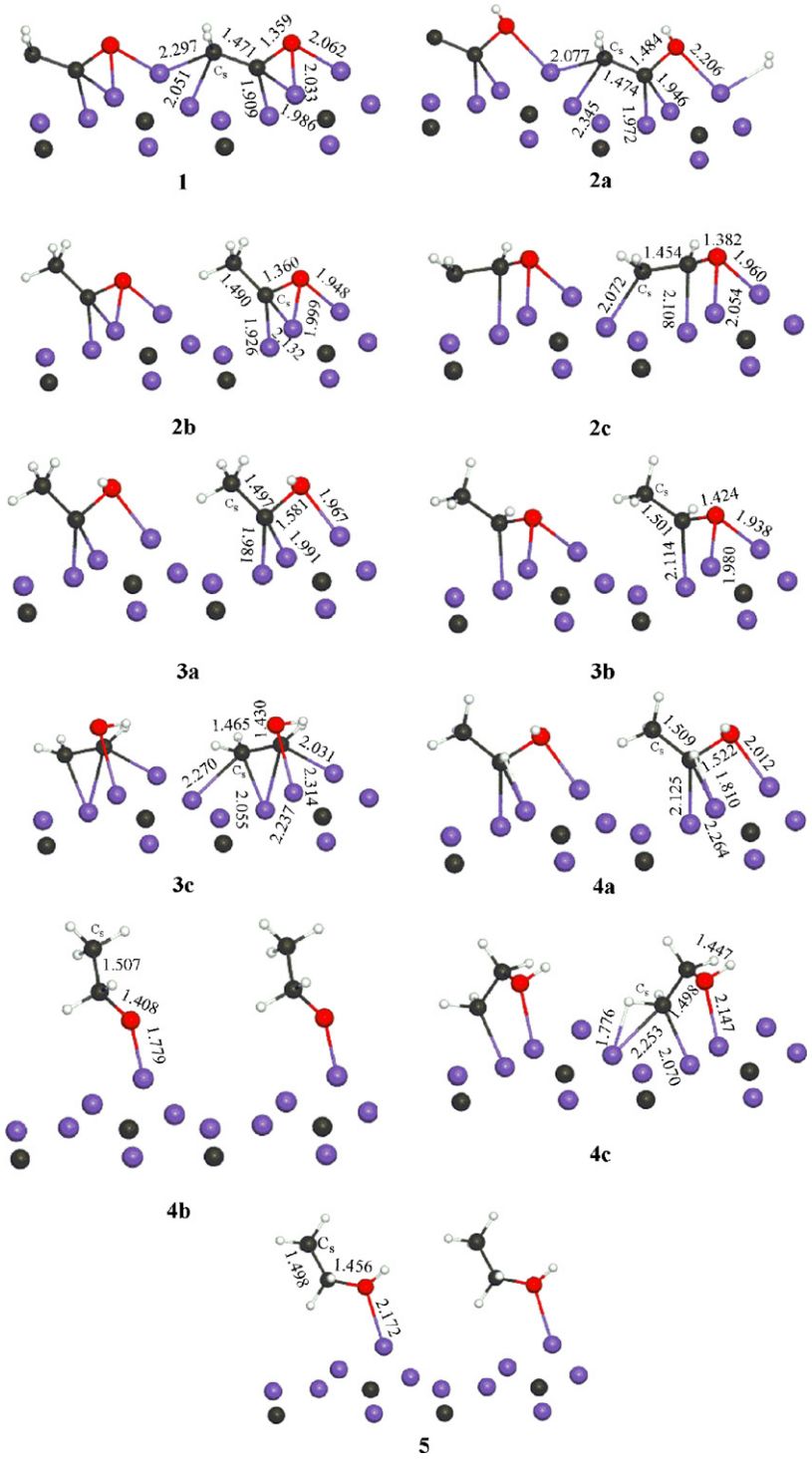

Fig. 3. The most stable adsorbed modes of oxygenated reactant, intermediate, and product (Fe/purple; C/gray; O/red and H/white). (For interpretation of the references to colour in this figure legend, the reader is referred to the web version of the article.)

are shown in dashed lines. In free **2a**, the frontier orbitals are the p_y orbital on the unsaturated carbon atom and the π^*_{CC} anti-bonding at about 3.5 eV, and they shift downward to about −4.5 and −2.2 eV after adsorption, respectively. In free **2b**, the frontier orbitals are the p_y orbital on the unsaturated carbon atom and the π^*_{CC}/π^*_{CO} anti-bonding at 2.3 eV, and they shift downward to about −4.0 and −2.2 eV after adsorption, respectively. The frontier orbitals of free **2c** are the π_{CO} and and p_y orbital and the π^*_{CC}/π^*_{CO} anti-bonding at about 4.7 eV, and they shift downwards to −4.0 and −2.1 eV after adsorption, respectively.

The LDOS of free and adsorbed CH_3COH (**3a**), CH_3CHO (**3b**), and CH_2CHOH (**3c**) are shown in Fig. 6. The valence bands of free **3a–c** in the singlet ground state are shown in dashed lines. In free **3a**, the frontier orbitals are the lone pair electron (n) and the π_{CC}/π^*_{CO} at 2.5 eV, and they shift downwards to about −4.7 and −2.1 eV after adsorption, respectively. In free **3b**, the

Table 1
Adsorption energies and binding modes of intermediates in ketene hydrogenation

Species	No.	ΔE_{ads}	Binding mode
Ketene (C_sH_2CO)	**1**	−2.41	η^3 (C_s, C, O)
Hydroxyvinyl (C_sH_2COH)	**2a**	−3.25	η^3 (C_s, C, O)
Acetyl (C_sH_3CO)	**2b**	−2.66	η^2 (C, O)
Formylmethyl (C_sH_2CHO)	**2c**	−2.43	η^3 (C_s, C, O)
Hydroxyethylidene (C_sH_3COH)	**3a**	−2.59	η^2 (C, O)
Acetaldehyde (C_sH_3CHO)	**3b**	−0.95	η^2 (C, O)
Hydroxyethylene (C_sH_2CHOH)	**3c**	−0.38	η^3 (C_s, C, O)
1-Hydroxyethyl (C_sH_3CHOH)	**4a**	−1.31	η^2 (C, O)
Ethoxy ($C_sH_3CH_2O$)	**4b**	−2.85	η^1 (O)
2-Hydroxyethyl ($C_sH_2CH_2OH$)	**4c**	−1.35	η^2 (C_s, O)
Ethanol ($C_sH_3CH_2OH$)	**5**	−0.51	η^1 (O)
Vinylidene (CC_sH_2)	**6**	−5.69	η^2 (C, C_s) (C, four-fold)
Ethylidyne (CC_sH_3)	**7a**	−6.17	η^1 (C) (C, four-fold)
	7a′	−5.83	η^1 (C) (C, three-fold)
Vinyl (CHC_sH_2)	**7b**	−3.00	η^2 (C, C_s) (CH, three-fold)
	7b′	−3.51	η^2 (C, C_s) (CH, four-fold)
Ethylidene (CHC_sH_3)	**8a**	−3.75	η^1 (C) (CH, three-fold)
Ethene ($CH_2C_sH_2$)	**8b**	−0.73	η^2 (C, C_s) (CH_2, C_sH_2, two-fold)
	8b′	−0.97	η^2 (C, C_s) (CH_2, C_sH_2, three-fold)
	8b″	−0.93	η^2 (C, C_s)
Ethyl ($CH_2C_sH_3$)	**9**	−1.61	η^1 (C) (CH_2, two-fold)
Ethane ($CH_3C_sH_3$)	**10**	−0.07	

frontier orbitals are the π_{CO} and the π^*_{CO} at about 3.8 eV, and they shift downwards to about −4.3 and −2.0 eV after adsorption, respectively. The frontier orbitals of free **3c** are the π_{CC}/π_{CO} and the π_{CC}/π^*_{CO} at 5.2 eV, and they shift to −4.7 and −3.3 eV after adsorption, respectively.

The LDOS of free and adsorbed CH_3CHOH (**4a**), CH_3CH_2O (**4b**), and CH_2CH_2OH (**4c**) are shown in Fig. 7. The valence bands of the isolated doublet ground state of **4**–**c** are shown in dashed lines. In free **4a**, the frontier orbitals are the p_z and the π^*_{CO} at 1.9 eV, and they shift downwards to −3.6 and −2.8 eV after adsorption, respectively. The frontier orbitals of free **4b** are the p_y and the π^*_{CO} at 1.2 eV, and they shift downwards to −4.3 and −2.5 eV after adsorption, respectively. In **4c**, the frontier orbitals are the p_z and the π^*_{CC} at about 2.4 eV, and they shift downwards to −4.3 and −3.4 eV after adsorption, respectively.

The LDOS of free and adsorbed CCH_2 (**6**) fragment are shown in Fig. 8a. In free **6**, the frontier orbitals are the lone pair p electron at the Fermi level and the π^*_{CC} at 3.1 eV, and they shift downwards to −3.8 and −2.4 eV after adsorption, respectively. The LDOS of free and adsorbed three-fold and four-fold CH_3C (**7**) are also shown in Fig. 8b and c. In free **7**, the frontier orbitals are the single occupied p_x orbital at the Fermi level and the π^*_{CC} at 2.7 eV, and they shift downwards to −3.7 and −2.7 eV after four-fold adsorption, respectively, and to −3.6 and −2.6 eV, after the three-fold adsorption.

In free CH_2CH, the frontier orbitals are the p_z at the Fermi level and the π^*_{CC} at about 4.7 eV. In the three-fold CH_2CH (**7b**) in Fig. 7d, the p_z and π^*_{CC} orbitals shift downwards to −3.7 and −2.8 eV, respectively. In the four-fold CH_2CH (**7b′**), the bands of the p_z and π^*_{CC} orbitals shift downwards to −4.0 and −2.8 eV, respectively.

The LDOS of free and adsorbed CH_3CH, CH_2CH_2 and CH_3CH_2 in dashed and solid lines are shown in Fig. 9. The frontier bands of free CH_3CH in the triplet ground state are two singly occupied orbitals p_y at −0.9 eV and p_z at the Fermi level and the $\sigma_{CH}/\sigma^*_{CC}$ at about 3.0 eV, and they shift downwards to −5.0, −3.7, and −2.3 eV in **8a**, respectively. The frontier orbitals of free CH_2CH_2 in the single ground state are the π'_{CC} at the Fermi level and the π^*_{CC} at about 5.7 eV, and they shift downward to −5.3 and −2.8 eV in **8b**, respectively. While, the π'_{CC} orbital and the π^*_{CC} orbital in **8b′** shift downward to −6.0 and −2.6 eV, respectively. The π'_{CC} orbital and the π^*_{CC} orbital in **8b″** shift downward to −4.7 and −0.9 eV, respectively. The frontier orbitals of free CH_3CH_2 in the doublet ground state are the single occupied p_y orbital at the Fermi level and the π^*_{CC} at about 2.3 eV, and they shifts downward to −4.0 and −2.1 eV in **9** after adsorption, respectively.

3.2. Reaction pathway

3.2.1. Ethanol formation

There are two three-fold sites for added H atom (**H** and **H′**), and their energy difference is only 0.06 eV. On the basis of their similar local structures, hydrogen migration from **H** to **H′** should be very easy. As shown in Fig. 10, there are two routes for H migration, the direct and the stepwise ways. The direct way has an energy barrier of 0.73 eV. In a transition state **TS(H/H′)**, H is adsorbed at the top site. In the stepwise way, H shifts from the three-fold site in **H** to another four-fold site (**Ha**), then, to the three-fold site (**Hb**), and finally to the three-fold site in **H′**. Within this process, **Ha** is the most stable adsorbed state, followed by **Hb** (0.12 eV) and **H′** (0.15 eV) and **H** (0.21 eV), respectively. The highest barrier is 0.21 eV from **Ha** to **Hb**. In transition states **TS(H/Ha)**, **TS(Ha/Hb)** and **TS(Hb/H′)**, H atom is adsorbed at a two-fold site. Thus, the stepwise way is more favorable kinetically. This agrees with the H migration on

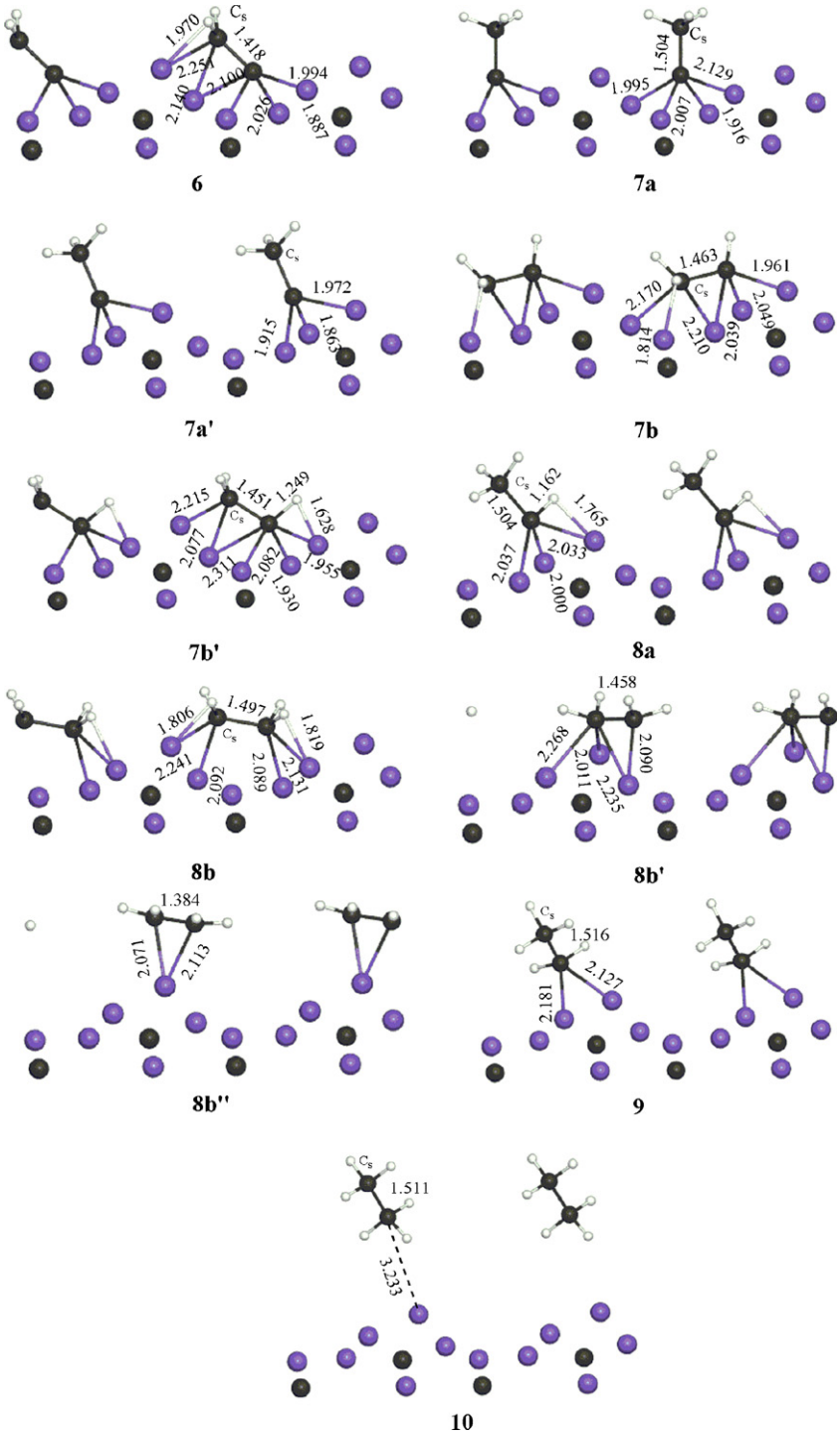

Fig. 4. The most stable adsorbed modes of hydrocarbons (Fe/purple; C/gray; O/red and H/white). (For interpretation of the references to colour in this figure legend, the reader is referred to the web version of the article.)

Fe(1 1 0), in which the energy barrier of H migration is 0.05 eV through a long-bridge site and 0.19 eV through a short-bridge site [48]. H migration on Fe(1 1 1) needs to overcome about 0.1 eV from the most favorable top-shallow bridge site to a quasi four-fold site [49].

The potential energy surface of all the pathways for ketene hydrogenation is shown in Fig. 11. The reaction pathway of ketene direct hydrogenation is shown by a blue line. In the first H addition step, the energy barrier from **1H** (co-adsorbed three-fold H and **1**) to **2a** is 1.79 eV. For **2b** formation, the energy barrier of **1H′** to **2b** is 1.07 eV. For **2c** formation, the energy barrier of **1H** to **2c** is 0.86 eV. The formation reactions of **2a–c** are endothermic by 0.96, 0.34, and 0.56 eV, respectively. Thus, the formation of **2b** and **2c** is more favorable than that of **2a** both thermodynamically and kinetically. Furthermore, the higher barrier and lower endothermicity of **2b**, and the lower barrier and

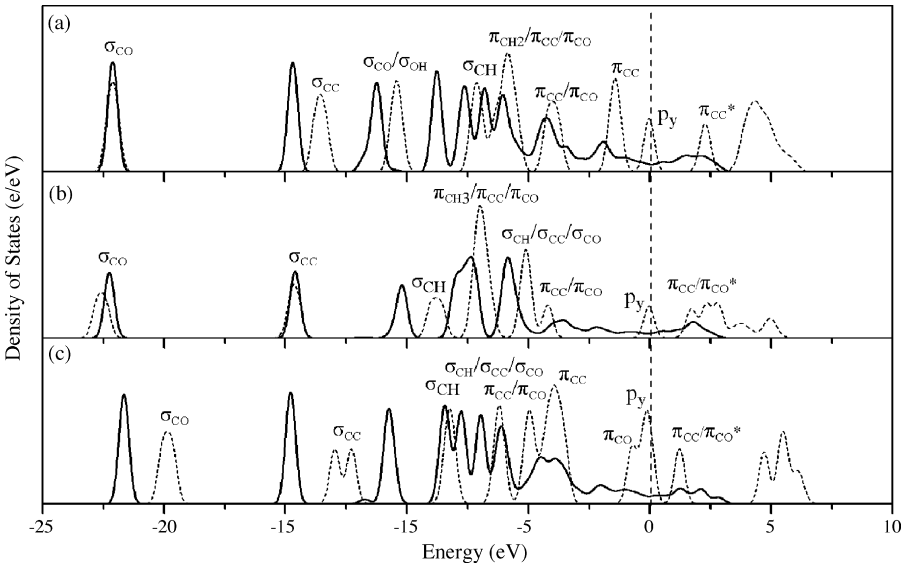

Fig. 5. LDOS of adsorbed C_sH_2COH (**2a**), C_sH_3CO (**2b**), C_sH_2CHO (**2c**) on $Fe_5C_2(0\,0\,1)$ are shown in (a)–(c), respectively (solid line for bands after adsorption; dashed line for bands before adsorption).

higher endothermicity of **2c** indicate that **2c** is favorable kinetically and **2b** is favorable thermodynamically. The rather lower barriers of their back reactions might reveal the possible interconversion between **2b** and **2c**. Indeed, **2b** was observed in ketene hydrogenation on Ru(0 0 1) at 200–250 K [18,19], and the ethanol formation on Rh–Fe/SiO_2 at 503 K [16] and on Rh/SiO_2 at 503–543 K [17].

In the second H addition step, the pathways from **2b** to **3a** and **3b** are both endothermic by 1.29 and 0.49 eV, and have energy barriers of 2.29 and 0.86 eV, respectively. As s result, **2b** hydrogenation favors the formation of **3b** instead of **3a** in thermodynamics and kinetics. Thermodynamically, **3b** is most stable, while **3a** and **3c** are 0.64 and 0.89 eV higher in energy, respectively.

For the pathway from **2c** to **3b** and **3c**, the energy barriers are 1.18 and 2.14 eV, respectively. In addition, the reactions from **2c** to **3b** and **3c** are also endothermic by 0.27 and 1.32 eV, respectively. It indicates that **3b** is much more favorable than that of **3c**. Therefore, **3b** is the main product in both thermodynamics and kinetics, while **3c** formation is rather difficult.

In the third H addition step, there are two pathways from **3b** to **4a** and **4b**. The calculated energy barrier for the pathway from **3b** to **4b** is 0.61 eV. Since the reaction from **3b** to **4a** is endothermic by 1.16 eV, the energy barrier of this reaction should be not

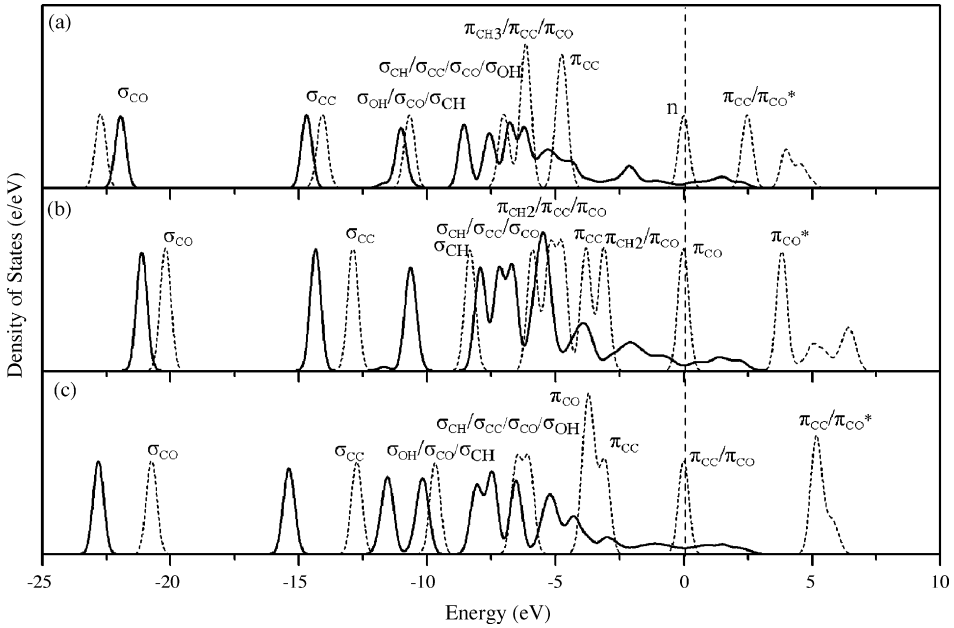

Fig. 6. LDOS of C_sH_3COH (**3a**), C_sH_3CHO (**3b**), C_sH_2CHOH (**3c**) on $Fe_5C_2(0\,0\,1)$ are shown in (a)–(c), respectively (solid line for bands after adsorption; dashed line for bands before adsorption).

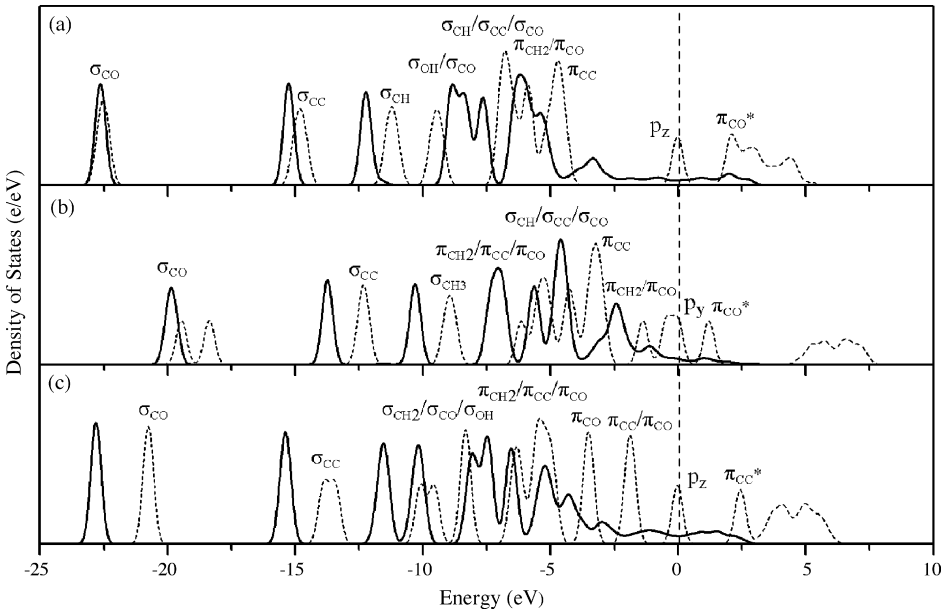

Fig. 7. LDOS of C_sH_3CHOH (**4a**), $C_sH_3CH_2O$ (**4b**), $C_sH_2CH_2OH$ (**4c**) on $Fe_5C_2(0\,0\,1)$ are shown in (a)–(c), respectively (solid line for bands after adsorption; dashed line for bands before adsorption).

less than this value. This means that the energy barrier from **3b** to **4a** is at least 0.55 eV higher than that from **3b** to **4b**. Thus, **4b** formation is more favorable than **4a** formation. Indeed, $C_sH_3CH_2O$ is observed in the process of ethanol formation on Rh–Fe/SiO_2 catalysts [16].

As mentioned above, **3b** is the main product of the second H addition step, while **3c** formation is not favorable. Furthermore, adsorbed **4b** is the most stable species thermodynamically, while adsorbed **4a** and **c** are highly in energy by 1.12 and 1.50 eV. Therefore, the pathways of **3c** to **4a** and **4c** are not

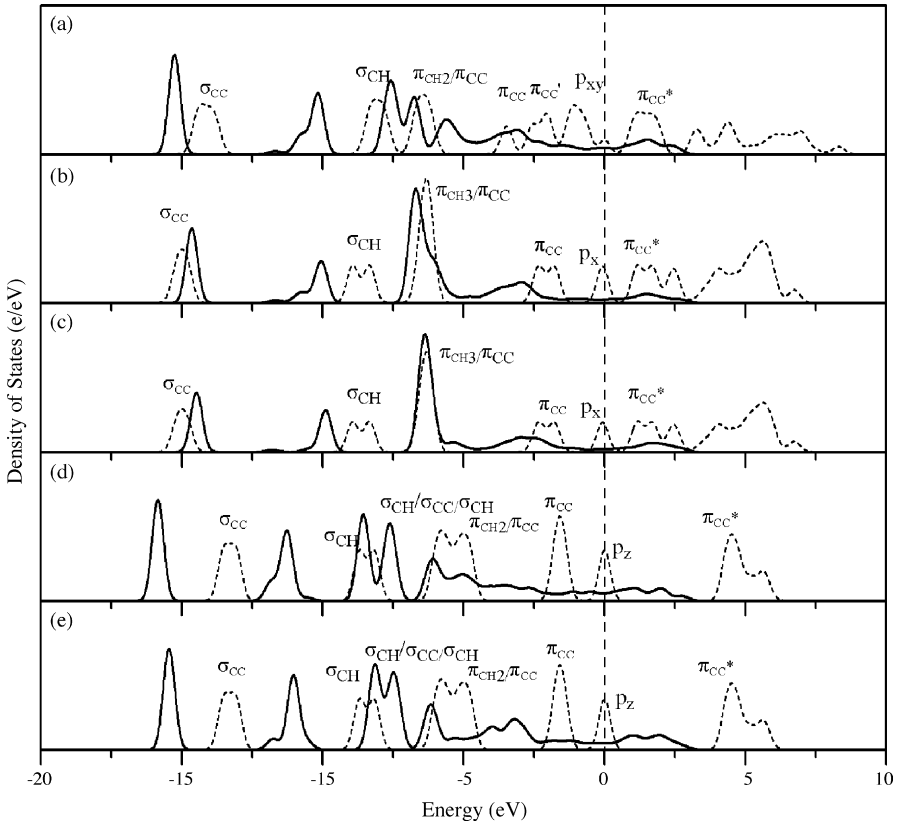

Fig. 8. LDOS of C_sH_2C (**6**), four-fold C_sH_3C (**7a**), three-fold C_sH_3C (**7a′**), three-fold C_sH_2CH (**7b**), and four-fold C_sH_2CH (**7b′**) on $Fe_5C_2(0\,0\,1)$ are shown in (a)–(e), respectively (solid line for bands after adsorption; dashed line for bands before adsorption).

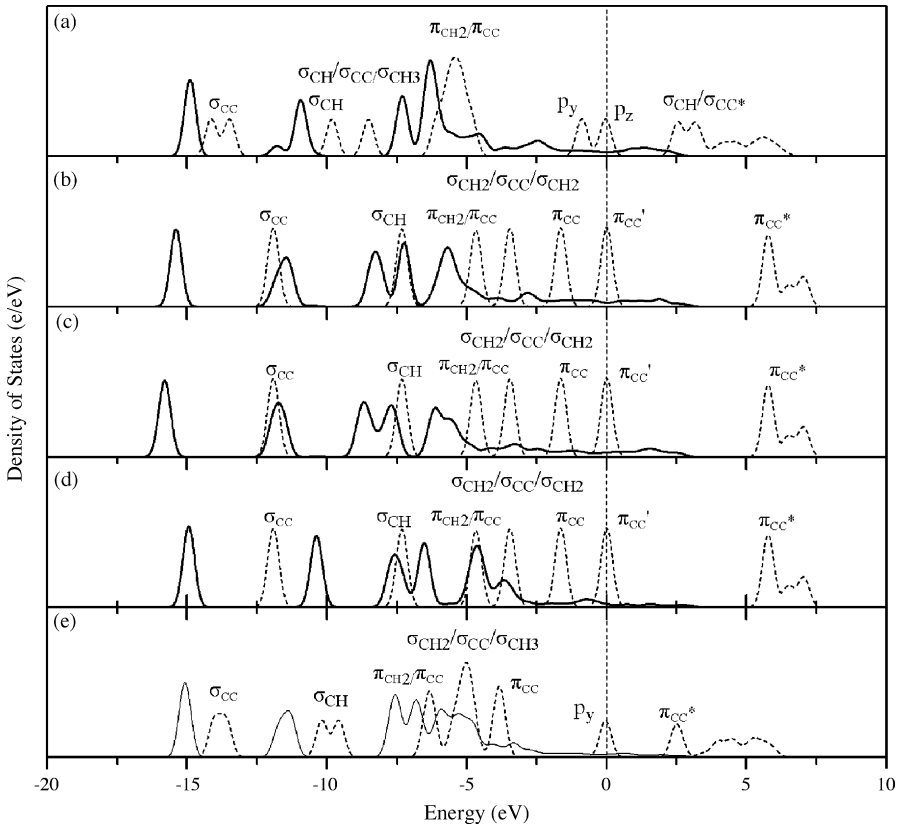

Fig. 9. LDOS of C_sH_3CH (**8a**), $C_sH_2CH_2$ (**8b**), $C_sH_2CH_2$ (**8b′**), $C_sH_2CH_2$ (**8b″**) and $C_sH_3CH_2$ (**9**) on $Fe_5C_2(0\,0\,1)$ are shown in (a)–(e), respectively (solid line for bands after adsorption; dashed line for bands before adsorption).

favorable. Comparatively, the pathway of **3a** to **4a** is endothermic by 0.36 eV, and has an energy barrier of 0.85 eV, which is 0.24 eV higher than that from **3b** to **4b**. Therefore, **4b** formation is most favorable in thermodynamics and kinetics.

In the last H addition step, **4b** hydrogenation leads to formation of **5**, and the energy barrier of this reaction is 1.42 eV. Similarly, Remediakis et al. [50] studied methanol formation from CO and H_2 on Ni(1 1 1) using the DFT method, and indicated that methanol is formed from formaldehyde (HCHO) and methoxy (CH_3O) hydrogenation. In addition, Davis et al. added ^{14}C labeled ethanol into syngas, and found that ethanol dehydrogenation results in acetaldehyde formation on iron-based catalysts in FTS [51]. Thus, on the $Fe_5C_2(0\,0\,1)$ surface, the main pathway for ethanol formation from ketene hydrogenation is C_sH_2CO (**1**) → [C_sH_3CO (**2b**) and/or C_sH_2CHO (**2c**)] → C_sH_3CHO (**3b**) → $C_sH_3CH_2O$ (**4b**) → $C_sH_3CH_2OH$ (**5**).

3.2.2. Dissociation of oxygenated intermediates

During ketene hydrogenation, C–O cleavage can occur and result in the formation of hydrocarbon. During ketene hydrogenation to ethanol, the most preferred intermediates are

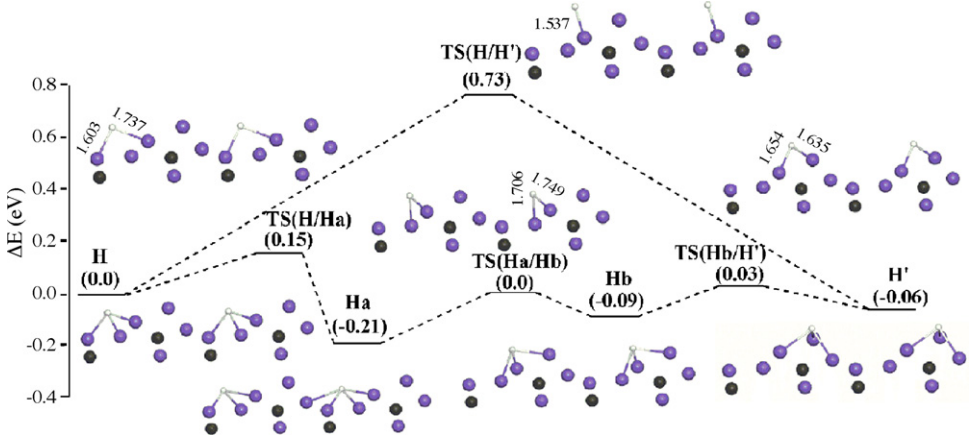

Fig. 10. H diffusion process of from three-fold **H** to three-fold **H′**.

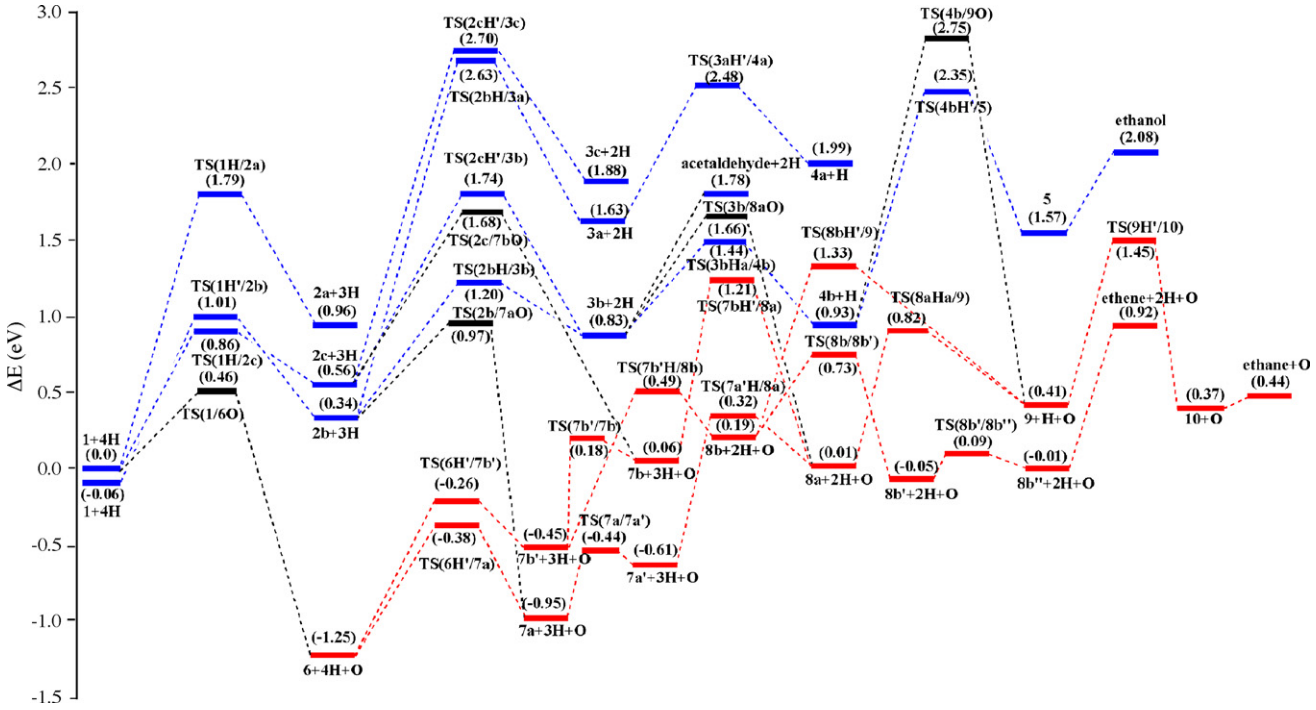

Fig. 11. Potential energy surface of the formation of oxygenates (blue line), and hydrocarbons (red line). (For interpretation of the references to colour in this figure legend, the reader is referred to the web version of the article.)

ketene (H_2C_s=C=O, **1**), acetyl (H_3C–C=O, **2b**), formylmethyl (H_2C_s–CHO, **2c**), acetaldehyde (H_3C_s–CHO, **3b**), and ethoxy (H_3C_s–CH_2O, **4b**), respectively. The dissociation reactions of these oxygenated intermediates are shown by black lines in Fig. 11.

C_sH_2CO (**1**) dissociation forms vinylidene (H_2C_sC, **6**) and a three-fold O atom. The dissociation of **1** is exothermic by 1.25 eV, and the energy barrier is 0.46 eV. C_sH_3CO (**2b**) dissociation forms co-adsorbed ethylidyne (CC_sH_3, **7a**) and a three-fold O atom exothermically by 1.29 eV, and the energy barrier is 0.63 eV. C_sH_2CHO (**2c**) dissociation forms the co-adsorbed vinyl (CHC_sH_2, **7b**) and a three-fold O atom exothermically by 0.50 eV, and has an energy barrier of 1.12 eV. C_sH_3CHO (**3b**) dissociates into ethylidene (CHC_sH_3, **8a**) and a three-fold O atom. The dissociation of **3b** has a barrier of 0.83 eV, and is exothermic by 0.82 eV. $C_sH_3CH_2O$ (**4b**) dissociates into ethyl ($CH_2C_sH_3$, **9**) and a three-fold O atom. The dissociation of **4b** has a barrier of 1.82 eV, and is exothermic by 0.52 eV.

Compared with their barriers for hydrogenation, the energy barriers of ketene (C_sH_2CO), acetyl (C_sH_3CO), and formylmethyl (C_sH_2CHO) dissociation on Fe_5C_2(0 0 1) are lower by 0.40, 0.23 and 0.06 eV, respectively. Consequently, vinylidene (CC_sH_2) formation is more favorable than that of either acetyl or formylmethyl, and the formation of ethylidyne (CC_sH_3) and vinyl (CHC_sH_2) is more favored than that of acetaldehyde. The energy barriers of C_sH_3CHO and $C_sH_3CH_2O$ dissociations are higher than those of their hydrogenation by 0.22 and 0.40 eV, respectively. Once acetaldehyde is formed, it is favorable to hydrogenation instead of dissociation.

Indeed, the yield of acetaldehyde is rather low in a typical composition of oxygenates in FTS products on the industrial Fe–Mn catalysts at 533 K [52]. It is related with desorption, hydrogenation, dehydrogenation and dissociation of acetaldehyde (**3b**). Desorption of **3b** needs 0.95 eV. Hydrogenation of **3b** to **4b** needs 0.61 eV, while that from **3b** to **2b** and **2c** needs 0.37 and 0.91 eV, respectively. The C–O cleavage of **3b** needs 0.83 eV. Therefore, **3b** hydrogenation, dehydrogenation is more favored than dissociation and desorption, resulting in the low yield of acetaldehyde.

3.2.3. *Ethene and ethane formation*

To compare with the dissociation of oxygenates, the reactions of hydrocarbons are investigated, and are also shown by red lines in Fig. 11. Ketene (**1**) dissociation can result in CC_sH_2 (**6**), and further hydrogenation of **6** leads to ethene and ethane. The hydrogenation of **6** forms CC_sH_3 (**7a**) and CHC_sH_2 (**7b′**). The energy barrier from **6** to **7a** is 0.87 eV, which is close to that of CCH_2 hydrogenation on Ru-steps (0.9 eV) [22]. The energy barrier from **6** to **7b′** is 0.99 eV.

H addition to **7a** forms CHC_sH_3 (**8a**), and **7b′** hydrogenation also forms CHC_sH_3 (**8a**) and $CH_2C_sH_2$ (**8b**). The pathway of **7a** to **8a** is a two-step reaction, and four-fold **7a** firstly shifts to three-fold **7a′**, then hydrogenation results in the formation of **8a**. The diffusion of CC_sH_3 from **7a** to **7a′** needs 0.51 eV. The energy barrier from **7a′** to **8a** is 0.93 eV. There are two pathways from **7b′** to **8a** and **8b**. The pathway from **7b′** to **8a** is a two-step reaction, and $CHCH_2$ firstly shifts from a four-fold site (**7b′**) to a three-fold site (**7b**), then its hydrogenation leads to $CHCH_3$ (**8a**). The energy barriers of these two reactions are 0.63 and 1.15 eV, respectively. The total energy barrier from **7b′** to **8a** is 1.66 eV. While the barrier from **7b′** to **8b** is 0.94 eV, and is much lower than that from **7b′** to **8a**. Therefore, **7b′** hydrogenation

is favorable to forming **8b** rather than to forming **8a**. This is in agreement with the fact that the hydrogenation of vinyl groups produces ethylene preferentially on Pt(1 1 1) [53]. Isomerization from **8a** (CH_3CH) to **8b** (CH_2CH_2) is also calculated, and the energy barrier is 2.53 eV. Thus, the pathway of **8b** formed by the isomerization of **8a** on Fe_5C_2(0 0 1) is not favorable.

8b is a di-σ adsorbed form, and needs to become π-adsorbed form for ethene desorption. **8b** first becomes another di-σ adsorbed form (**8b′**), then the π-adsorbed form (**8b″**), and finally desorbs. The energy barriers of **8b** to **8b′** and **8b′** to **8b″** are 0.54 and 0.14 eV, respectively. In contrast, ethene desorption needs a higher barrier of 0.93 eV.

H addition to CHC_sH_3 (**8a**) and $CH_2C_sH_2$ (**8b**) forms $CH_2C_sH_3$ (**9**). The pathway from **8a** to **9** has an energy barrier of 0.81 eV. The pathway from **8b** to **9** has an energy barrier of 1.14 eV. Comparatively, the barrier for ethene (**8b**) desorption of 0.93 eV is lower than that of its hydrogenation (1.14 eV), indicating that ethene (**8b**) prefers desorption rather than further hydrogenation to ethane. In addition, the re-adsorption of ethene in FTS is very important in giving the increase in the higher hydrocarbons yield [54,55,32]. H addition to $CH_2C_sH_3$ (**9**) yields $CH_3C_sH_3$ (**10**). The calculated energy barrier from **9** to **10** is 1.04 eV.

Analyzing the calculated results of the three sections, we find that the energy barrier of ketene (C_sH_2CO) dissociation into vinylidene (C_sH_2C) on Fe_5C_2(0 0 1) is 0.40 eV lower than its hydrogenation in the first step, and this indicates that the oxygenated intermediate can produce hydrocarbons. The consequence of further hydrogenation is the formation of hydrocarbons rather than oxygenated products. This is in line with the experimental observation [20,21]. During both ketene hydrogenation and dissociation, the carbon vacancies are generated on the surface. The activity of carbon vacancy is related with the ratio of Ti and C atoms on the TiC(1 0 0) surfaces [56]. For the Fe_5C_2(0 0 1) surface, the ratio of Fe and C exposed on the surface is 5:1. CO is strongly activated, and H_2 is dissociated on the Fe_5C_2(0 0 1) surface [9,44]. However, the carbon vacancies formed by surface carbon hydrogenation are really not free vacancies, because they are covered by the newly formed species. The properties of these free vacancies need further detailed studies.

4. Conclusion

The detailed reaction mechanism of ketene hydrogenation on the Fe_5C_2(0 0 1) surface was studied with the DFT method. This is because that ketene is one of the most important intermediates on the surface under the co-adsorption of H_2 and CO. The main formation pathway of ethene is C_sH_2CO (**1**) → CC_sH_2 (**6**) → CHC_sH_2 (**7b′**) → $CH_2C_sH_2$ (**8b**), while that of ethane is C_sH_2CO (**1**) → CC_sH_2 (**6**) → CC_sH_3 (**7a**) → CC_sH_3 (**7a′**) → CHC_sH_3 (**8a**) → $CH_2C_sH_3$ (**9**) → $CH_3C_sH_3$ (**10**). Comparatively, ketene sequential hydrogenation to ethanol follows the main pathway of C_sH_2CO (**1**) → [C_sH_3CO (**2b**) and/or C_sH_2CHO (**2c**)] → C_sH_3CHO (**3b**) → $C_sH_3CH_2O$ (**4b**) → $C_sH_3CH_2OH$ (**5**). Importantly, the energy barrier of ketene (C_sH_2CO) dissociation on Fe_5C_2(0 0 1) is lower by 0.40 eV than its hydrogenation. As a result, ketene dissociation with the formation of hydrocarbons is more favorable than the stepwise hydrogenation with the formation of ethanol. The expected product should be hydrocarbons rather than ethanol.

Acknowledgments

This work was supported by Chinese Academy of Science and the National Nature Foundation of China (20473111 and 20590361); and the National Outstanding Young Scientists Foundation of China (No. 20625620).

Appendix A. Supplementary data

Supplementary data associated with this article can be found, in the online version, at doi:10.1016/j.molcata.2007.03.057.

References

[1] F. Fischer, H. Tropsch, Brennstoff-Chem. 7 (1926) 97.
[2] F. Fischer, H. Tropsch, Chem. Ber. 59 (1926) 830.
[3] H. Pichler, H. Schulz, Chem. Ind. Technol. 42 (1970) 1162.
[4] J.T. Kummer, P.H. Emmett, J. Am. Chem. Soc. 5 (1953) 5177.
[5] J.B. Berziger, R.J. Madix, J. Catal. 65 (1980) 36.
[6] A. Takeuchi, J.R. Katzer, J. Catal. 82 (1983) 477.
[7] P.M. Loggenberg, L. Carlton, R.G. Copperthwaite, G.J. Hutchings, J. Chem. Soc., Chem. Commun. (1987) 541.
[8] J.W. Kolis, E.M. Holt, D.F. Shriver, J. Am. Chem. Soc. 105 (1983) 7307.
[9] D.-B. Cao, F.-Q. Zhang, Y.-W. Li, H. Jiao, J. Phys. Chem. B 108 (2004) 9094.
[10] D.-B. Cao, F.-Q. Zhang, Y.-W. Li, J. Wang, H. Jiao, J. Phys. Chem. B 109 (2005) 10922.
[11] W. Wu, Z. Wu, C. Liang, X. Chen, P. Ying, C. Li, J. Phys. Chem. B 107 (2003) 7088.
[12] J. Ren, C.-F. Huo, J.G. Wang, Y.-W. Li, H. Jiao, Surf. Sci. 596 (2005) 212.
[13] R.J. Daroda, J.R. Blackborow, G. Wilkinson, J. Chem. Soc., Chem. Commun. (1980) 1098.
[14] A. Takeuchi, J.R. Katzer, J. Phys. Chem. 86 (1982) 2438.
[15] A. Deluzarche, J.-P. Hindermann, R. Kieffer, R. Breault, A. Kienemann, J. Phys. Chem. 88 (1984) 4993.
[16] T. Fukushima, H. Arakawa, M. Ichikawa, J. Phys. Chem. 89 (1985) 4440.
[17] H. Arakawa, T. Fukushima, M. Ichikawa, K. Takeuchi, T. Matsuzaki, Y. Sugi, Chem. Lett. (1985) 23.
[18] M.A. Henderson, P.L. Radloff, J.M. White, C.A. Mims, J. Phys. Chem. 92 (1988) 4111.
[19] M.A. Henderson, P.L. Radloff, C.M. Greenlief, J.M. White, C.A. Mims, J. Phys. Chem. 92 (1988) 4120.
[20] H.G. Stenger Jr., C.N. Satterfield, Ind. Eng. Chem. Process. Des. Dev. 24 (1985) 411.
[21] H.G. Stenger Jr., C.F. Askonas, Ind. Eng. Chem. Fundam. 25 (1986) 410.
[22] Z.-P. Liu, P. Hu, J. Am. Chem. Soc. 124 (2002) 11568.
[23] C. Zheng, Y. Apeloig, R. Hoffmann, J. Am. Chem. Soc. 110 (1988) 749.
[24] Q. Ge, M. Neurock, H.A. Wright, N. Srinivasan, J. Phys. Chem. B 106 (2002) 2826.
[25] A. Alcalá, M. Mavrikakis, J.A. Dumesic, J. Catal. 218 (2003) 178.
[26] C.A. Mims, L.E. McCandlish, M.T. Melchior, Catal. Lett. 1 (1988) 121.
[27] N.W. Cant, A.T. Bell, J. Catal. 73 (1982) 257.
[28] C.A. Mims, J.J. Krajewski, K.D. Rose, M.T. Melchior, Catal. Lett. 7 (1990) 119.
[29] M.L. Turner, P.K. Byers, H.C. Long, P.M. Maitlis, J. Am. Chem. Soc. 115 (1993) 4417.
[30] M.L. Turner, H.C. Long, A. Shenton, P.K. Byers, P.M. Maitlis, Chem. Eur. J. 1 (1995) 549.

[31] P.M. Maitlis, H.C. Long, R. Quyoum, M.L. Turner, Z.-Q. Wang, J. Chem. Soc., Chem. Commun. (1996) 1.
[32] D.S. Jordan, A.T. Bell, J. Phys. Chem. 90 (1986) 4797.
[33] F.A.P. Cavalcanti, R. Oukaci, I. Wender, D.G. Blackmond, J. Catal. 123 (1990) 270.
[34] M.C. Payne, D.C. Allan, T.A. Arias, J.D. Joannopoulos, Rev. Mod. Phys. 64 (1992) 1045.
[35] V. Milman, B. Winkler, J.A. White, C.J. Pickard, M.C. Payne, E.V. Akhmataskaya, R.H. Nobes, Int. J. Quantum Chem. 77 (2000) 895.
[36] J.P. Perdew, A. Zunger, Phys. Rev. B 23 (1981) 5048.
[37] J.P. Perdew, J.A. Chevary, S.H. Vosko, K.A. Jackson, M.R. Pederson, D.J. Singh, C. Fiolhais, Phys. Rev. B 46 (1992) 6671.
[38] D. Vanderbilt, Phys. Rev. B 41 (1990) 7892.
[39] H.J. Monkhorst, J.D. Pack, Phys. Rev. B 13 (1976) 5188.
[40] S.G. Louie, S. Froyen, M.L. Cohen, Phys. Rev. B 26 (1982) 1738.
[41] G. Le Caer, A. Simon, A. Lorenzo, J.M. Genin, Phys. Stat. Solid A 6 (1971) K97.
[42] T.A. Halgren, W.N. Lipscomb, Chem. Phys. Lett. 49 (1977) 225.
[43] S. Immel, Molarch+, MOLecular ARCHlitecture Modeling Programm V7.05, Technical University of Darmstadt, Darmstadt, Germany, 2002.
[44] D.-B. Cao, F.-Q. Zhang, Y.-W. Li, J. Wang, H. Jiao, J. Phys. Chem. B 109 (2005) 833.
[45] D. Fruchart, et al., in: H.P.J. Wijn (Ed.), Crystal and Solid State Physics, LandoltBornstein, vol. 19c, Springer-Verlag, Berlin, 1988, p. 24.
[46] J. Silvestre, R. Hoffmann, Langmuir 1 (1985) 621.
[47] G.W. Watson, R.P.K. Wells, D.J. Willock, G.J. Hutching, J. Phys. Chem. B 104 (2000) 6439.
[48] D.E. Jiang, E.A. Carter, Surf. Sci. 547 (2003) 85.
[49] C.-F. Huo, Y.-W. Li, J. Wang, H. Jiao, J. Phys. Chem. B 109 (2005) 14160.
[50] I.N. Remediakis, F.A. Abild-Pedersen, J.K. Nørskov, J. Phys. Chem. B 108 (2004) 14535.
[51] L.-M. Tau, R. Robinson, R.D. Ross, B.H. Davis, J. Catal. 105 (1987) 335.
[52] B.-T. Teng, C.-H. Zhang, J. Yang, D.-B. Cao, J. Chang, H.-W. Xiang, Y.-W. Li, Fuel 84 (2005) 791.
[53] Z.-M. Liu, X.-L. Zhou, D.A. Buchanan, J. Kiss, J.M. White, J. Am. Chem. Soc. 114 (1992) 2031.
[54] E. Iglesia, S.C. Reyes, R.J. Madon, J. Catal. 129 (1991) 238.
[55] T. Komaya, A.T. Bell, J. Catal. 146 (1994) 237.
[56] S.A. Jansen, R. Hoffmann, Surf. Sci. 197 (1988) 474.